Supporting Information for

Facet-dependent Peroxo Species Regulate Product Distribution and H_2O_2 Utilization in CeO_2-catalyzed Aniline Oxidation

Linyuan Tian,[1#] Yin-Song Liao,[2,3#] Jyh-Pin Chou,[4*] Zicong Tan,[1] Jian Lin Chen,[5] Jung-Hoon Lee,[6*] Tsz Woon Benedict Lo[7] and Yung-Kang Peng[1,8*]

[1]Department of Chemistry, City University of Hong Kong, Hong Kong SAR.
[2]Department of Materials Science and Engineering, National Tsing Hua University, Hsinchu 300, Taiwan.
[3]Tsing Hua Interdisciplinary Program, National Tsing Hua University, Hsinchu 300, Taiwan.
[4]Department and Graduate Institute of Physics, National Changhua University of Education, Changhua 500, Taiwan.
[5]Department of Applied Science, School of Science and Technology, Hong Kong Metropolitan University, Hong Kong SAR.
[6]Department of Chemistry, Soonchunhyang University, Asan 31538, Korea.
[7]Department of Applied Biology and Chemical Technology, The Hong Kong Polytechnic University, Hong Kong SAR.
[8]City University of Hong Kong Chengdu Research Institute, Chengdu, China.
[#]These authors contributed equally to this work

[*]Correspondence: ykpeng@cityu.edu.hk; jhlee67@sch.ac.kr; jpchou@cc.ncue.edu.tw

Catalyst Preparation

CeO_2 cube and rod were prepared by a hydrothermal method. For CeO_2 cube, 0.651 g of $Ce(NO_3)_3 \cdot 6H_2O$ and 3.6 g of NaOH were added to 30 ml H_2O and then stirred for 30 minutes; CeO_2 rod was prepared as the same procedure but 7.2 g NaOH was used. The mixture was heated in Teflon-lined stainless steel under 180 °C and 100 °C for 24 hours, respectively. For CeO_2 octa., 0.8141 g of $Ce(NO_3)_3 \cdot 6H_2O$ and 0.7005 g of hexamethylenetetramine were added to 110 mL H_2O and stirred for 3 hours at 75 ºC. All catalysts were collected by centrifugation and washed with ethanol for 5 times and then calcined at 200 °C before use.

Catalytic testing

H_2O_2 decomposition on CeO_2. 5 mL methanol containing 7.5 mg of CeO_2 and 2.25 mmol H_2O_2 was stirred at room temperature for 25 hours. To measure the residual H_2O_2, the solution collected at a specific time point was centrifuged at 14000 rpm for 4 mins to remove CeO_2. 100 µL of the upper solution was mixed with 1.9 mL methanol for tracking the progress of H_2O_2 decomposition by UV-vis spectroscopy at 240 nm ($\varepsilon_{240} = 39.4\ M^{-1}\ cm^{-1}$). **Figure S4** shows the calibration line established using a series of H_2O_2 solution with known concentration.

Michaelis-Menten kinetic analysis. Using methanol as solvent, 2 mL CeO_2 (0.8 mg/mL) was mixed with 2 mL H_2O_2 solution with concentration of 10, 20, 40, 60, 80, 100, 160, 200, 300 mM in room temperature. Then, the initial rate ($V_{initial}$) can be obtained by the decrease of H_2O_2 concentration revealed by UV-vis spectroscopy at 240 nm in the given time. The corresponding maximum velocity (V_{max}) can be obtained from the Michaelis-Menten equation below. The K_m is the substrate concentration (or H_2O_2 concentration) where the initial reaction rate reaches 50% of its V_{max}.

$$V_{initial} = \frac{V_{max} \times [H_2O_2]}{K_m + [H_2O_2]}$$

In-situ Raman Measurements. 4 mg of CeO_2 was placed on the glass slide in square (2 mm × 2 mm). The Raman spectra was recorded at 0, 2, 5, and 8 mins after the addition of 4 µL of H_2O_2 (5 M, methanol as solvent).

Aniline Oxidation with H_2O_2. 1.5 mmol aniline, 7.5 mg CeO_2, and 2.25 mmol H_2O_2 were added to 5 mL of methanol. Solution collected at each time point was centrifuged at 14000 rpm for 5 min to remove CeO_2 followed by product analysis by GC-MS (Agilent 5890, column, 30 m × 0.25 mm ×0.25µm) and GC (Agilent 6890, column-TG-5SilMS, 30 m × 0.25 mm ×0.25 µm). The concentration of each product in the solution was determined by integrating the area of their peak and comparing these areas with commercial references. The conversion of aniline, and yield/selectivity of products can be calculated by equations below (n= 1 for nitrosobenzene and nitrobenzene, n=2 for azoxybenzene)[1]:

$$Conv. = \frac{\sum n \times mole\ of\ product_x}{initial\ moles\ of\ aniline} \times 100\%$$

$$Sel._x = \frac{n \times mole\ of\ product\ x}{\sum n \times mole\ of\ product_x} \times 100\%$$

$$Yield_x = Conv. \times Sel._x$$

Density functional theory (DFT) calculation

The density functional theoretical calculations were conducted by using Vienna *Ab-initio* Simulation Package (VASP)[2, 3]. The electron-ion interaction was described within the projected augmented wave method (PAW)[4] with cut-off energy of 460 eV, while the exchange-correlation functional was performed using generalized gradient approximation proposed by Perdew, Burke, and Ernzerhof[5]. The Hubbard U correction (DFT+U) was employed, with a specific strength of 3.5 eV for the delocalized f-orbital of cerium atom. Brillouin zone sampling was performed using a 4 × 4 × 4 *k*-mesh for the primitive cell, where the optimized lattice constant was 3.885 Å. All the relaxations were conducted with an electronic self-consistent loop criterion of 10^{-5} eV. We constructed 6-layered 5 × 5 supercell models of the (100), (110), and (111) surface with a vacuum thickness greater than 20Å. All atoms except for the bottom three layers, which were fixed to bulk geometry, were allowed to relax freely. We obtained the adsorption energy (E_{ad}) using the following equation:

$$E_{ad} = E_{total} - E_{surface} - \mu$$

where the E_{total}, $E_{surface}$, and μ correspond to the total energy of the adsorbed system, bare surfaces, and chemical potential of adsorbates. To evaluate the reaction energy barriers, we implemented the climbing image nudge-elastic band method with the force-based optimizer, fast inertial relaxation engine (FIRE)[6].

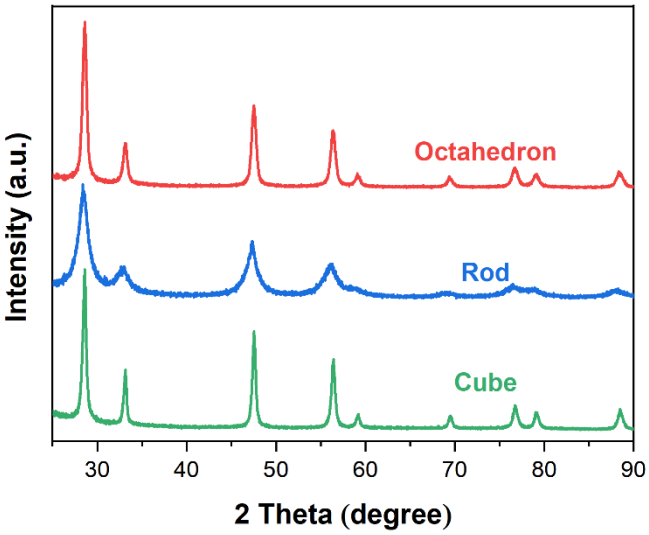

Figure S1. XRD patterns of CeO_2 samples.

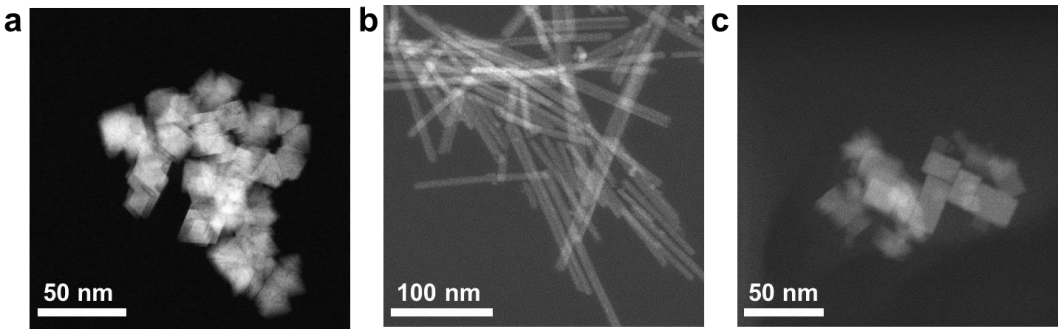

Figure S2. Annular dark-field STEM images of CeO_2 (a) octa., (b) rod, and (c) cube.

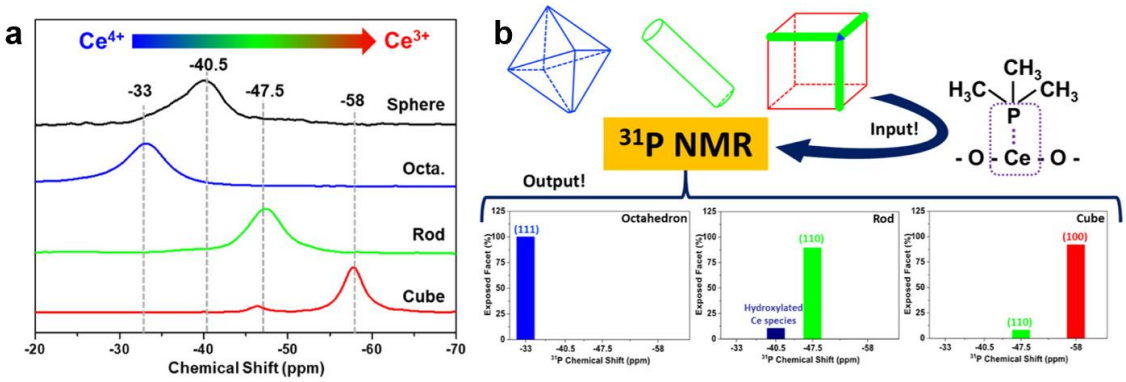

Figure S3. (a) TMP-^{31}P NMR spectra of CeO_2 morphologies, (b) information (i.e., chemical state, distribution, and concentration of surface Ce species) extracted from the deconvoluted TMP-^{31}P NMR spectra of CeO_2 morphologies.[7] Reproduced with permission from *ACS publisher*.

In our recent report, trimethylphosphine (TMP) was used as a ^{31}P nuclear magnetic resonance (NMR) probe for the study of Ce chemical state among CeO_2 surfaces.[7] TMP, a Lewis base molecule, can coordinate to a surface coordinated unsaturated metal cation (Lewis acid, LA) and span a wide δ^{31}P range of -20 to -60 ppm in ^{31}P NMR. δ^{31}P of this TMP-LA adduct can be used to differentiate cations with various LA strengths on facets because a strong surface LA site will form a stronger chemical bond with TMP and shift δ^{31}P to positive ppm. CeO_2 nanocrystallites in the shape of octahedron, rod, and cube were thus examined by this TMP-^{31}P NMR technique. As shown in the **Figure S3a**, the distribution of the Ce chemical state is shape-dependent with decreasing δ^{31}P of TMP-Ce adducts: -33 ppm for octahedron > -47.5 ppm for rod > -58 ppm for cube. DFT calculation was also employed to correlate the δ^{31}P with their dominant surface (i.e., (111) for octahedron, (110) for rod, and (100) for cube). The distribution of facets for CeO_2 octahedron, rod, and cube was concluded in **Figure S3b**. For the octahedron sample, the only signal with high symmetry at -33 ppm confirms the well-defined (111) surface. Unfortunately, the trace amount of the (100) surface believed at the tips of this shape cannot be observed in the ^{31}P NMR spectrum at around -58 ppm. For the rod sample, no signal at -33 and -58 ppm but an extra broad shoulder at -40.5 ppm suggests no detectable (111) and (100) facet exposure and that ~10% of surface Ce atoms are hydroxylated Ce species (similar to a sphere surface). For the cube sample, the peak area of the extra signal at -47.5 ppm further suggests that 8% surface Ce is hosted by the (110) facet at cube edges, matching well with the molecular dynamic prediction of the (110)/(100) ratio in the CeO_2 cube (~10%).[8] Since three shapes are all enclosed ≥ 90% by their dominant surface, we only consider one surface for each morphology herein to simplify the study on the role of their Ce coordination structures in aniline oxidation.

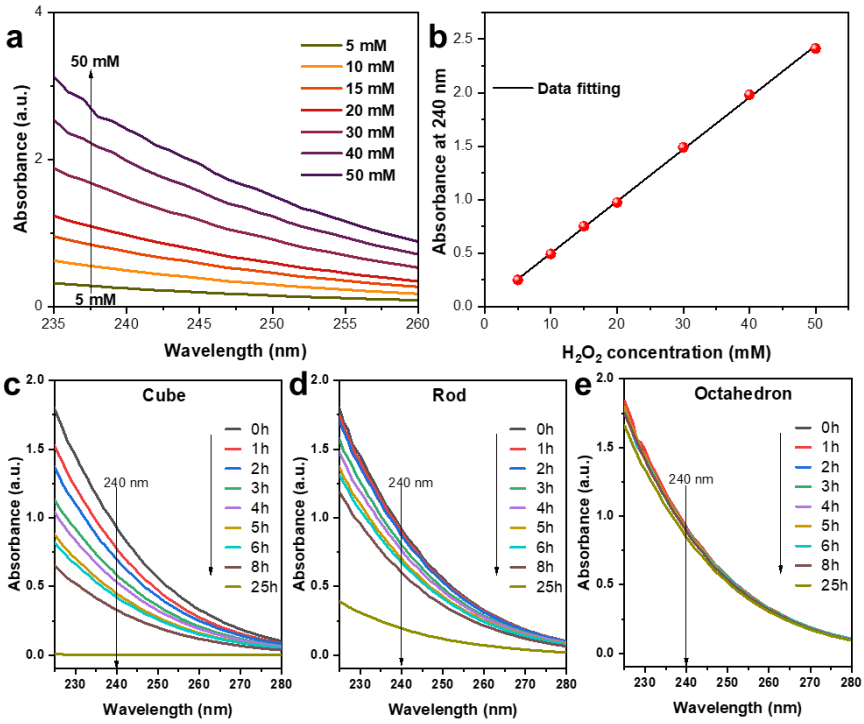

Figure S4. (a) UV-Vis spectral of H_2O_2 with different concentrations and (b) the corresponding calibration curve of absorbance at 240 nm and H_2O_2 concentrations. (c-e) UV-vis spectral of H_2O_2 decrease on cube, rod, and octahedron without aniline. Reaction condition: 5 mL methanol containing 7.5 mg of CeO_2 and 2.25 mmol H_2O_2 was stirred at room temperature.

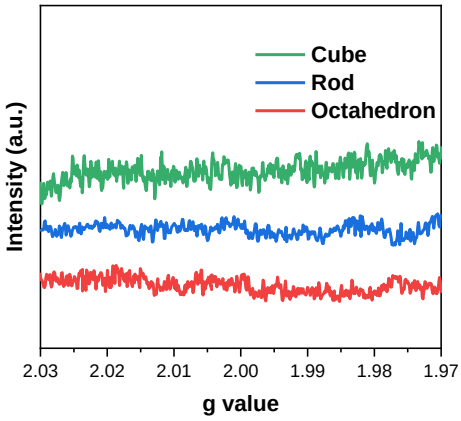

Figure S5. Electron paramagnetic resonance (EPR) results of CeO_2 samples and no signal of surface oxygen vacancy-associated Ce sites (g = 2.00) was found. This result is consistent with the literature that this signal should appear only when pristine CeO_2 is reduced or doped with foreign atoms.[9-11]

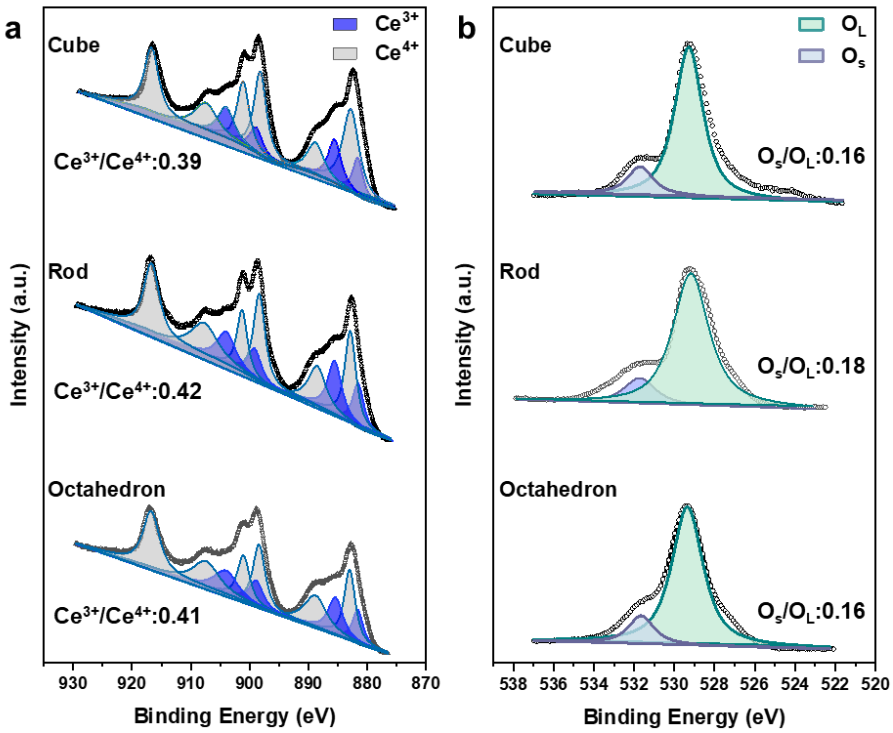

Figure S6. The deconvoluted XPS spectra of CeO_2 samples in (a) Ce_{3d} and (b) O_{1s} regions.

The similar Ce^{3+}/Ce^{4+} ratio obtained among CeO_2 samples suggests that this factor should also play a negligible role in the selective H_2O_2 activation. Note that the XPS Ce^{3+} signal here can be attribute to the abundant coordinated unsaturated Ce sites on crystal surface **(Scheme 1d)**. The quantity of surface OH groups was approached from the corresponding XPS O_{1s} range. Accordingly, all shapes exhibit a main peak of lattice oxygens (O_L) at 529.6 eV and a shoulder peak of surface O-relevant species (O_S) at 531.7 eV with a similar O_S/O_L ratio. This, together with the negligible oxygen vacancy-associated Ce sites revealed by EPR **(Figure S5)**, suggests that CeO_2 shapes bear a comparable amount of surface OH groups, which again cannot account for their extreme results in H_2O_2 activation.

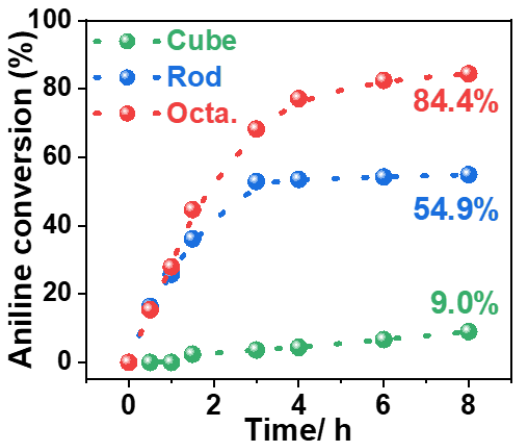

Figure S7. The time-dependent overall aniline conversion for CeO_2 samples.

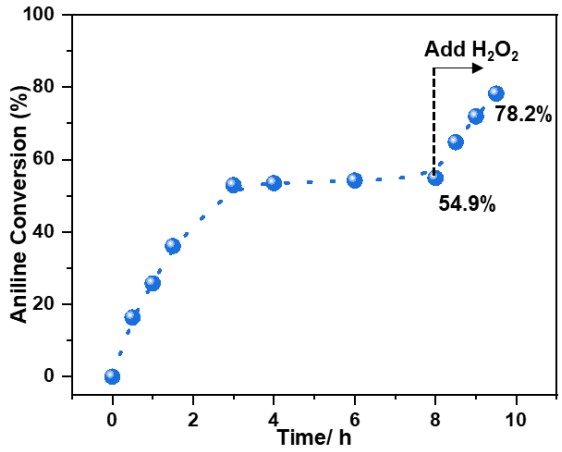

Figure S8. The conversion of aniline over CeO_2 rod with time. The reaction continues upon the addition of 2 mmol H_2O_2 at 8 hours of reaction.

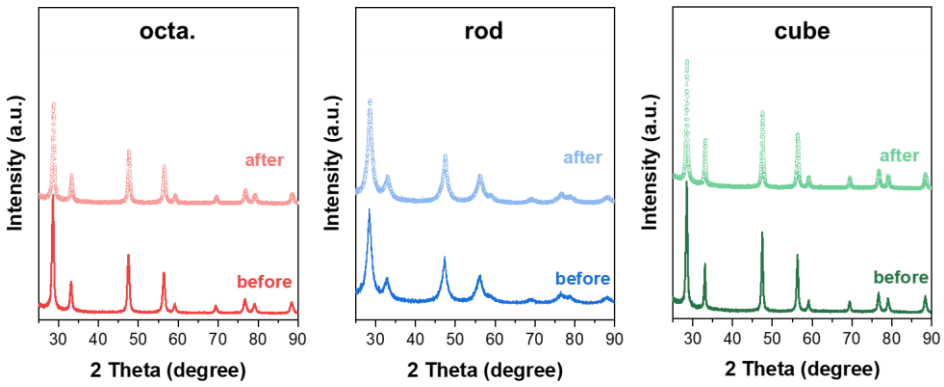

Figure S9. XRD patterns of CeO_2 samples before and after the reaction.

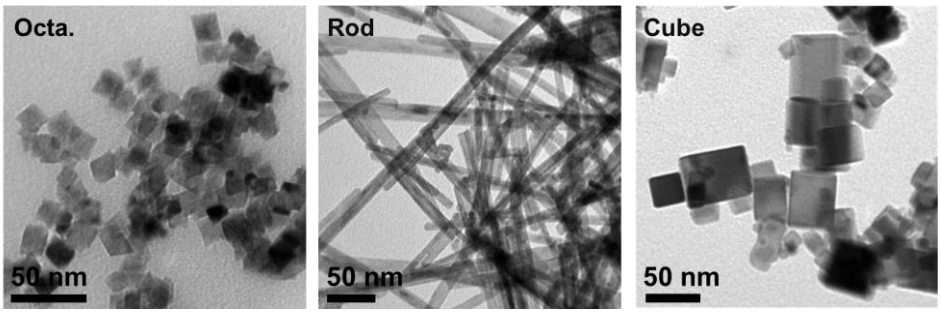

Figure S10. TEM images of the spent CeO_2 samples.

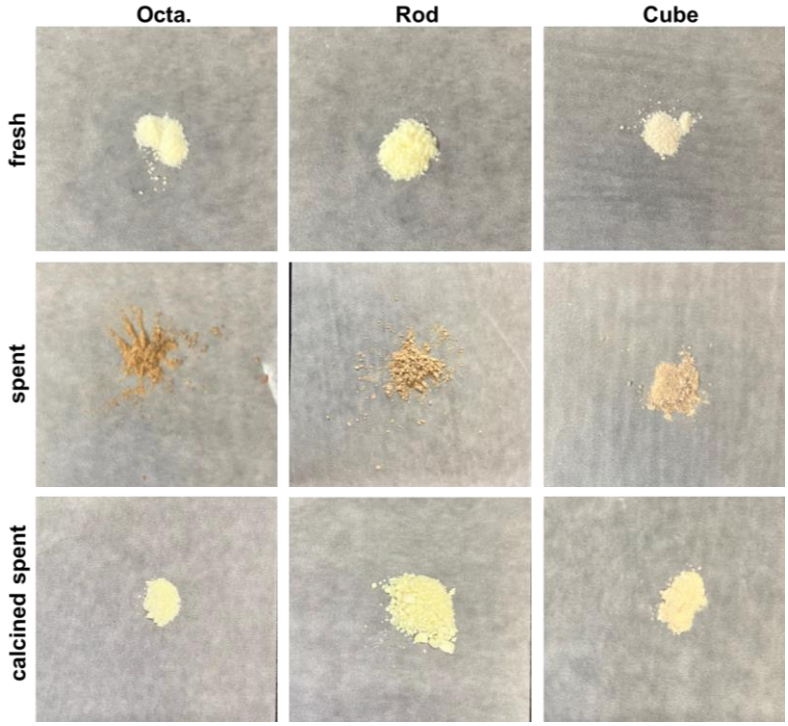

Figure S11. Digital photos of the (a) fresh, (b) spent, and (c) calcined spent CeO_2 samples.

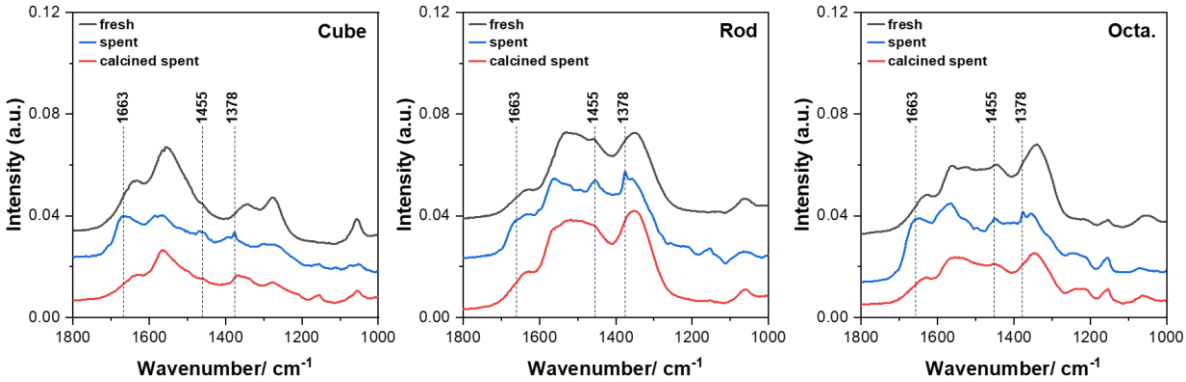

Figure S12 Infrared spectra of the fresh (black line), spent (blue line), and calcined spent (red line) CeO_2 samples. The adsorption of N-relevant species during the reaction can be supported by the emerging infrared (IR) signals of N=O stretching at 1455 and 1378 cm^{-1} for the spent CeO_2 samples.[12] Although the origin of the IR signal at 1663 cm^{-1} is still unknown, these N-relevant species can be removed by calcinating at 200°C as evidenced by the disappearance of these IR signals for the calcined spent samples.

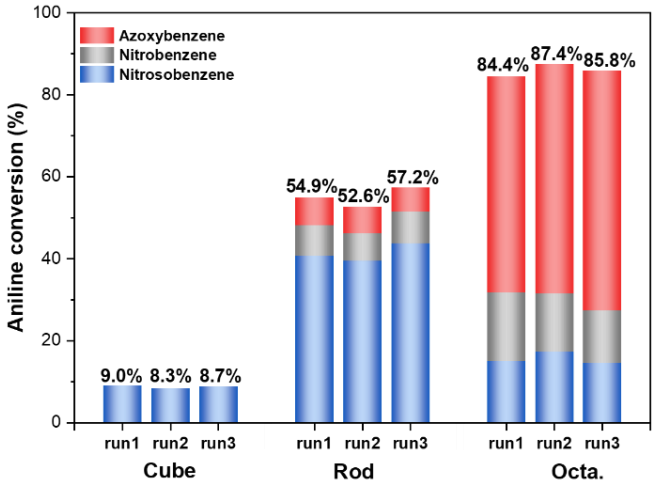

Figure S13. Aniline conversion and product distribution for CeO_2 samples in three runs.

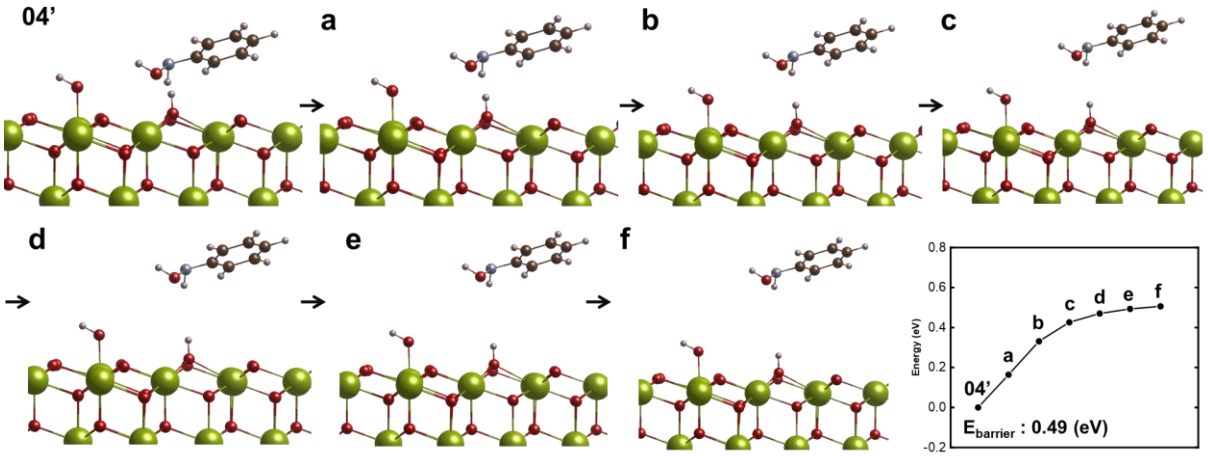

Figure S14. Re-optimized state 4 for the calculation of the desorption energy required for Ph-NHOH on (111) surface.

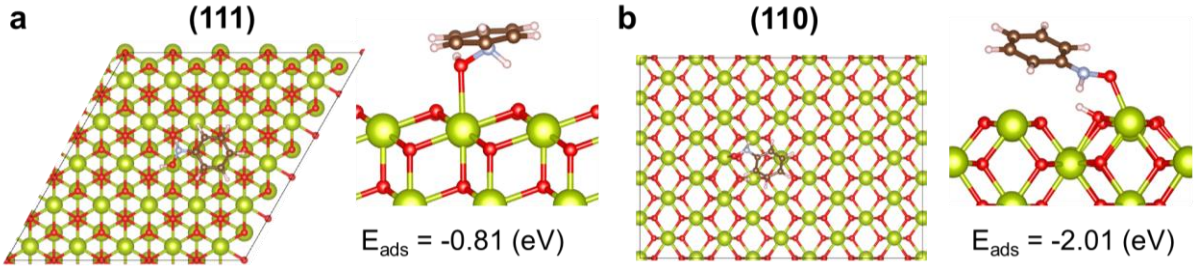

Figure S15. The adsorption of Ph-NHOH on CeO_2 (a) (111) and (b) (110) surfaces.

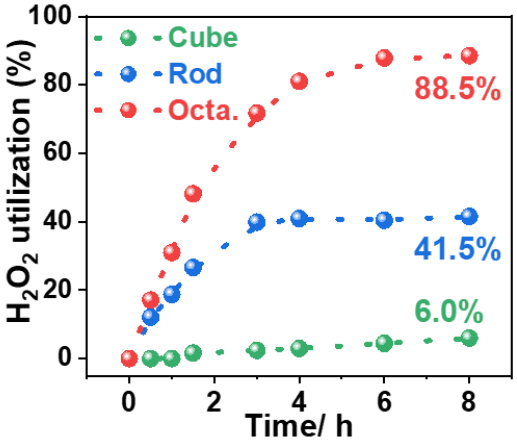

Figure S16. H_2O_2 utilization for CeO_2 samples as a function of time.

According to **Scheme 3**, aniline was found to be oxidized by HO_2 radicals to give nitrosobenzene as the sole product on the (100) surface. Since HO_2 radicals are generated by the oxidation of H_2O_2 by OH radicals, the production of nitrosobenzene thus consumes two H_2O_2. The utilization of H_2O_2 for the cube sample is thus calculated as (2* moles of nitrosobenzene)/initial moles of H_2O_2. As for the (111) surface, one end-on peroxo species specifically oxidize aniline to produce one Ph-NHOH. The further oxidation of Ph-NHOH to nitrosobenzene will consume one more H_2O_2. Since nitrosobenzene involves in 1) condensation reaction with Ph-NHOH to produce azoxybenzene and 2) oxidation reaction by another end-on peroxo species to give nitrobenzene. Given this, the utilization of H_2O_2 for the octa. sample was calculated as (2* moles of nitrosobenzene + 2*moles of azoxybenzene + 3*moles of nitrobenzene)/initial moles of H_2O_2. As for the (110) surface, aniline is directly oxidized by the side-on peroxo species to give nitrosobenzene. The production of one nitrosobenzene thus only requires one H_2O_2 on this surface. Since nitrosobenzene can be further oxidized to nitrobenzene by another side-on peroxo species, the generation of nitrobenzene thus needs two H_2O_2. Given that our rod sample is not perfectly enclosed by (110) surface (see ^{31}P NMR spectrum in **Figure S3**), the tiny amount of azoxybenzene observed for this sample should be attributed to the presence of hydroxylated Ce sites (~10%) on (111) surface. Therefore, the utilization of H_2O_2 is equal to (1* moles of nitrosobenzene + 2*moles of nitrobenzene + 2*moles of azoxybenzene)/initial moles of H_2O_2.

Table S1. The condensation of Ph-NHOH and nitrosobenzene at room temperature in the absence and presence of CeO_2 samples [Reaction condition: 5 mg CeO_2, 0.1 mmol Ph-NHOH, 0.1 mmol nitrosobenzene, 5 mL methanol, 30 minutes, room temperature].

Entry	Catalyst	Time (h)	Reaction	Conversion of Ph-NHOH
1	—	0.5	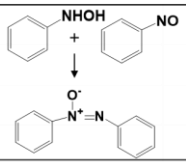	>95%
2	Cube	0.5		>95%
3	Rod	0.5		>95%
4	Octa.	0.5		>95%

References:

1. Y. Tao, B. Singh, V. Jindal, Z. Tang and P. P. Pescarmona, *Green Chem.*, 2019, **21**, 5852-5864.
2. G. Kresse and J. Furthmüller, *Phys. Rev. B*, 1996, **54**, 11169.
3. G. Kresse and J. Furthmüller, *Comput. Mater. Sci.*, 1996, **6**, 15-50.
4. G. Kresse and D. Joubert, *Phys. Rev. B*, 1999, **59**, 1758.
5. J. P. Perdew, K. Burke and M. Ernzerhof, *Phys. Rev. Lett.*, 1996, **77**, 3865.
6. E. Bitzek, P. Koskinen, F. Gähler, M. Moseler and P. Gumbsch, *Phys. Rev. Lett.*, 2006, **97**, 170201.
7. Z. Tan, G. Li, H.-L. Chou, Y. Li, X. Yi, A. H. Mahadi, A. Zheng, S. C. Edman Tsang and Y. K. Peng, *ACS Catal.*, 2020, **10**, 4003-4011.
8. U. Castanet, C. Feral-Martin, A. Demourgues, R. L. Neale, D. C. Sayle, F. Caddeo, J. M. Flitcroft, R. Caygill, B. J. Pointon, M. Molinari and J. Majimel, ACS Appl. Mater. Interfaces, 2019, **11**, 11384.
9. Y. Ding, L. Huang, J. Zhang, A. Guan, Q. Wang, L. Qian, L. Zhang and G. Zheng, *J. Mater. Chem. A*, 2020, **8**, 7229-7234.
10. Y. Ji, M. Yang, W. Cheng, C. Li and X. Liu, *Energy Adv.*, 2022, **1**, 868-871.
11. Z. Li, Z. Deng, L. Ouyang, X. Fan, L. Zhang, S. Sun, Q. Liu, A. A. Alshehri, Y. Luo and Q. Kong, *Nano Res.*, 2022, **15**, 8914-8921.
12. D. Combita, P. Concepción and A. Corma, *J. Catal.*, 2014, **311**, 339-349.